

# Printed Sensing: Assessing 3D-Printed Electrodes for Measuring Electrodermal Activity

Martin Schmitz  
Saarland University  
Saarbrücken, Germany  
mschmitz@cs.uni-saarland.de

Henning Klagemann  
Technical University of Darmstadt  
Darmstadt, Germany  
henning.klagemann@stud.tu-darmstadt.de

Dominik Schön  
Technical University of Darmstadt  
Darmstadt, Germany  
schoen@tk.tu-darmstadt.de

Thomas Kosch  
HU Berlin  
Berlin, Germany  
thomas.kosch@hu-berlin.de

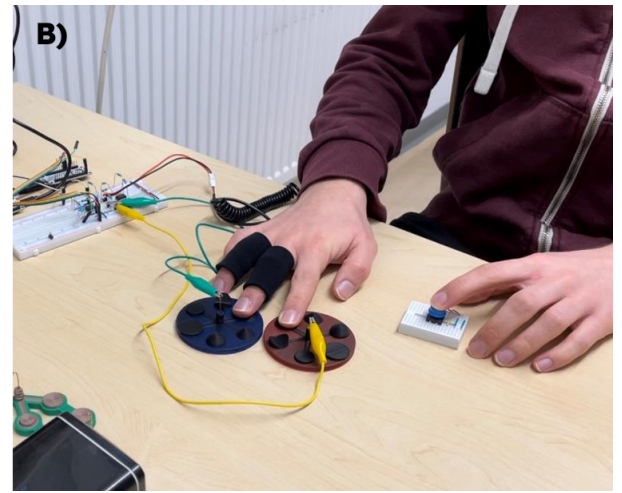
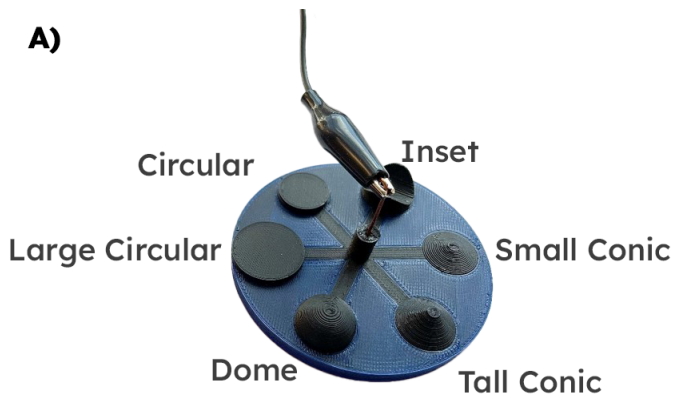


**Figure 1:** We evaluate the sensing efficiency of 3D-printed electrodes for measuring Electrodermal Activity (EDA). A) We compare different electrode sizes and shapes to a commercially available EDA device. B) Participants were conducting an auditory oddball task using our 3D-printed electrodes with regular electrodes functioning as ground truth. The participants were instructed to press a button when they perceived a specific sound.

## ABSTRACT

Electrodermal activity (EDA) reflects changes in skin conductance, closely tied to human psychological states. EDA sensors can assess stress, cognitive workload, arousal, and activity related to the parasympathetic nervous system used in various human-computer interaction applications. Yet, current limitations involve the complex attachment and proper skin contact with EDA sensors. This paper explores the novel concept of 3D printing electrodes for EDA measurements, potentially integrating sensors into arbitrary 3D printed objects, alleviating the need for complex assembly and attachment. We examine the adaptation of conventional EDA circuits for 3D-printed electrodes, assessing different electrode shapes and their impact on the sensing accuracy. A user study ( $N=6$ ) revealed that 3D-printed electrodes can measure EDA with similar accuracy while recommending larger contact areas for improved precision. We discuss design implications to facilitate EDA sensor integration into 3D-printed devices, fostering a diverse integration into everyday items using consumer-grade 3D printers for physiological interface prototyping.

## CCS CONCEPTS

• Human-centered computing → Empirical studies in HCI.

## KEYWORDS

Electrodermal Activity, Physiological Sensing, 3D Printing

## 1 INTRODUCTION

Electrodermal Activity (EDA) sensors play an important role in measuring skin sweat, offering valuable insights into the psychophysiological states of users, such as stress [5, 37] or mental workload [20]. The sympathetic nervous system [14] dynamically adjusts sweat secretion in response to psychological conditions, allowing the inference of a user's mental state [19, 38]. For instance, a sudden loud noise rapidly increases skin sweat, activating a “fight-or-flight” response [14]. EDA sensors detect such changes by applying electrodes with small voltages to the skin (i.e., typically on the fingers [4]) and assessing its resistance, which decreases with higher sweat conductivity. Sensing EDA has greatly interested the Human-Computer Interaction (HCI) community to implicitly assess user

states, such as mental workload [20], stress [21], or emotions [34]. Such measures can be used as implicit metrics for assessing user experience [19] or providing adaptive user interfaces [8]. Yet, the practical integration of EDA into user interfaces remains a challenge. While commercial devices are affordable, they require attaching electrodes to the user (i.e., to the fingers or feet), hindering the comfort and user acceptance of using EDA in interactive applications. While previous work showed that electrodes could be integrated into common skin contact points, such as VR controllers [7], such integrations are lavishly and only cover specific use cases, demanding a more flexible approach to sense EDA in everyday and common interaction scenarios. In addition, depending on where such electrodes are integrated into a 3D object, they will also have different shapes, possibly changing their sensing characteristics.

This paper, therefore, explores the feasibility of 3D printing EDA sensors to overcome these challenges and embed them seamlessly into everyday objects. To this end, we evaluate the suitability of differently shaped 3D-printed conductive electrodes for measuring EDA (see Figure 1). We contribute a user study that compares the measured values for different electrode shapes with commercially available EDA sensors for six participants performing an auditory oddball task. Our results show that certain shapes achieve a solid correlation with the commercial EDA sensor, while other shapes show a low correlation. Based on the results, we discuss the effects of electrode shapes and materials on accuracy and conclude with design suggestions for integrating physiological EDA sensing into 3D-printed objects.

## 2 RELATED WORK

Our work is rooted in sensing and using EDA for interactive applications. We, therefore, summarize related works in sensing EDA, 3D-printed physiological sensors, using EDA for interactive applications.

### 2.1 Sensing Electrodermal Activity

The terminology and framework presented in Boucsein’s work [6] constitute the foundation of EDA measurements. Boucsein’s work summarizes how EDA works and offers detailed insights into various EDA applications. The methodology aligns with the recommendations proposed by Fowles et al. [12] and the subsequent 2012 report from the Society for Psychophysiological Research Ad Hoc Committee on Electrodermal Measures [11]. These guidelines inform our approach to measuring EDA and interpreting the resulting data in this research. In this context, recent EDA research has been dedicated to developing recording devices suitable for unobtrusive and ambulatory use outside traditional laboratory and medical settings [1, 9, 28, 29, 32]. These studies focus on creating EDA sensors with minimal hardware requirements, often utilizing small sensor chips. An emphasis is placed on affordability, enabling long-term measurements, and maintaining a certain measurement quality. Many works focus on wearable devices, such as wristbands and smartwatches, with considerations for alternative recording sites to enhance user comfort and acceptability [15].

### 2.2 3D-Printed Sensors

Extensive research has been conducted and continues in 3D-printed sensor structures. Xu et al. [40] conducted a comprehensive review, encompassing recent examples of sensors measuring physical variables such as temperature and pressure, interactive tactile and strain sensors, and physiological sensors including EEG sensors. Furthermore, Dijkschoorn et al. have provided a detailed overview of techniques employed in the 3D printing sensor structures [10]. For example, 3D-printed sensors can provide touch detection on customized objects [23, 24].

Despite previous research, 3D-printed EDA sensors were rarely the objective of past research. Zhao et al. [41] demonstrated the feasibility of creating a fully printed EDA sensor chip using graphene ink for wrist attachment. However, this comes with challenges such as material specificity and shape limitations, utilizing a rectangular electrode shape of 16 mm<sup>2</sup>. Ho et al. focused on 3D printing electrodes, utilizing high-resolution powder bed printing for flexible, conductive structures in wearable sensors [13]. They created interconnected porous structures using sugar grains as powder, requiring coating and optional conductive material filling. While their approach showed promising results for various physiological sensors, including EDA, it involves intricate steps. Further investigations are necessary, especially using FDM printing for easy integration into arbitrary objects.

Numerous studies investigate 3D printed electrodes, yet they typically fall into two categories: those that generally analyze 3D printed electrodes for electrochemical sensing, utilizing methods such as Fused Deposition Modeling (FDM) and electrodeposition [16, 30], and those that concentrate on specific sensors, employing techniques such as FDM [39] or PolyJet printing [31]. Alsharif et al. recently reviewed 3D-printed electrodes, specifically those not reliant on electrolytic gels [2]. When applying electrodes for EDA, insights from conventional EDA electrodes, primarily silver chloride electrodes, can be employed. Studies on these electrodes highlight the correlation between the size of the contact area and measured skin conductance. Mahon and Iacono [22] observed a linear increase in the Skin Conductivity Level (SCL) and Skin Conductivity Response (SCR) amplitudes with a larger contact area. Thus, the electrode shape has an influence on the sensing quality.

### 2.3 Using Electrodermal Activity for Interactive Applications

Previous HCI studies investigated EDA for interactive applications. For instance, Pan et al. [26] proposed utilizing Orienting Responses as an “implicit communication paradigm,” employing SCR to indicate interruptions during audio stream consumption. Kosch et al. [19] demonstrated the utility of EDA as a measure for adaptive augmented reality production assistance systems. Shi et al. [33] examined EDA as a cognitive load indicator in traffic control management tasks, correlating higher SCLs with increased task complexity. Klarkowski et al. [18] explored the relationship between challenges in video games and EDA to enhance player experience. Furthermore, EDA is frequently passively recorded for subsequent analysis. Ayzenberg et al. [3] developed a system to implicitly log users’ stress levels during daily social interactions on mobile phones, aiming to

aid users in recalling and managing stressful situations. Additionally, EDA is employed to capture emotional states, as demonstrated by Kim et al. [17], who designed glasses equipped with an EDA sensor to track emotions during story reading. However, with the emerging number of applications for interactive EDA, it becomes increasingly important to ensure scientifically correct EDA measures. Babaei et al. [4] summarized previous research for interactive EDA, stated critique regarding their sensing approach, and provided directions on how the HCI community should assess EDA measures in the future.

Previous research showed that EDA can be used for interactive applications. Yet, integrating EDA electrodes into everyday objects remains a research challenge. In this work, we assess the measurement performance of customizable 3D-printed electrodes. Inspired by previous work looking at EDA electrode shapes [22], we compare the EDA measurement efficiency of different 3D-printed shapes.

### 3 EFFICIENCY OF 3D-PRINTED ELECTRODE SHAPE ON EDA MEASUREMENTS

We compare the EDA sensing performance of 3D-printed and commercially available EDA electrodes. We manipulate the electrode shape of the 3D-printed electrodes.

#### 3.1 Study Setup

To evaluate the impact of electrode shape on measurement outcomes, we utilized 3D printing to create a diverse set of six electrode pairs (see Figure 1). While most commercially available electrodes are typically circular, we also printed flat circular electrodes. Additionally, we produced electrodes with a larger diameter (“Large Circular”) to investigate the influence of electrode area. To explore the use of non-flat, sloped electrodes, we printed four additional pairs, including a pair with a spherical shape (“Dome”). Two electrodes were conical with flattened tips and varying heights, creating one pair with a more pointed configuration than the other. The final sloped electrodes were not curved outward but inward (“Inset”), providing the added benefit of guiding fingers intuitively to the correct location. When printed, these electrodes were printed using Protopasta Conductive PLA<sup>1</sup>, a composite material containing PLA, a dispersant, and carbon black, with a conductivity of up to 3.3 S/m (approximately 30  $\Omega$ /cm).

As a reference, we use the commercially available nickel dry Grove EDA Sensor by Seeed Technology<sup>2</sup>, which are circular and 15 mm in diameter. Therefore, all Protopasta electrodes, except the large circular ones, were printed with the same diameter. The electrodes were 3D printed using an Original Prusa i3 MK3S printer with Multi Material Upgrade 2S (MMU2S), and the layer height was set to 0.2 mm with 100% infill density using the rectilinear fill pattern from PrusaSlicer. All pipes had a cross-section of 4 mm  $\times$  4 mm and a length of 32.5 mm, extending from the outer end of the electrode to the center point of the board, where a lead was inserted into a cylinder printed on top of the pipes by heating the lead with a soldering iron.

To evaluate the performance of 3D-printed EDA sensors, it is also necessary to adapt existing EDA sensor circuits for compatibility with 3D-printed electrodes. More advanced signal processing tasks such as amplification and filtering can be optionally added as supplementary hardware components or executed through software. We intentionally focus on exosomatic recording using Direct Current (DC) [6], since it is most suitable approach for seamlessly integrating an EDA sensor into small objects. This approach eliminates the need for a reference electrode at a remote location and avoids the handling of Alternate Current (AC), for example by using a DC-to-AC converter.

#### 3.2 Method

We compare the shape and material of different 3D filaments with realistic EDA electrodes. We utilize an oddball task, where brief tones are repeatedly presented audibly to the participant, with certain tones having different frequencies, referred to as oddballs [36]. Initially employed to evoke a P300, a common feature in neuroscience studies [27], an event-related potential originating in the brain detectable through electroencephalography when an oddball is perceived. This task has been observed to also induce SCRs concurrently with the P300 known from neuroscience [25, 35]. Thus, the oddball task is well-suited for eliciting SCRs. While numerous tasks exist for triggering EDA, these specific ones are utilized in this study. It is important to note that they should be treated separately from assessing implicit EDA, denoting variations in skin conductance that are not intentionally provoked by a stimulus. The study employs a within-subjects design.

**3.2.1 Independent Variables.** We investigate the electrode shape as single independent variable. We simultaneously compare these to the Seeed Grove EDA electrode measurements during the oddball task. To that end, we created six shapes for the Protopasta conductive material (i.e., small conic, tall conic, circular, dome, large circular, circular, inset, see Figure 1).

**3.2.2 Dependent Variables.** We measure the skin conductivity from the 3D-printed and the commercially available Grove EDA sensor. The conductivity is measured in Siemens, a common measure for electrical conductivity. The conductivity of the 3D-printed and Grove sensor is measured at the same time. The sampling rate is synchronized between both sensors.

#### 3.3 Procedure & Task

The study involved six individuals (three females, three males). These volunteers were aged between 20 and 24 years, with a mean age of 22 (SD = 1.3). Two participants had reported consuming caffeine within the six hours preceding their involvement. The environmental conditions during the study were maintained at an average temperature of 21.4  $^{\circ}$ C (SD = 1.3) and an average humidity of 45.4% (SD = 2.8%). We complied to the recommendations by Babaei et al. [4] for conducting EDA studies. Upon arrival, participants were instructed to wash their hands with cold water. Subsequently, they sat at a table where the sensor and test electrodes were positioned. Detailed information about the study procedure and data

<sup>1</sup><https://proto-pasta.com/pages/conductive-pla> – last accessed 2024-01-25

<sup>2</sup>[https://wiki.seeedstudio.com/Grove-GSR\\_Sensor](https://wiki.seeedstudio.com/Grove-GSR_Sensor) – last accessed 2024-01-25

**Table 1: Pearson correlations between the different electrode shapes and the commercial EDA sensor. Bold values indicate the highest correlations.**

Electrode	Circular	Large Circular	Dome	Tall Conic	Small Conic	Inset
Pearson's r	.651	<b>.683</b>	.279	<b>.680</b>	.331	.597

collection was provided to them. Following the explanation, participants signed their informed consent and were directed to place reference electrodes on their non-dominant hands.

The electrode connected to the positive potential of the twin EDA sensor was affixed to the middle phalanx of the middle finger, while the other electrode was attached to the middle phalanx of the ring finger. No electrolyte gel was used, as its application cannot be assumed for the specific type of EDA sensors under investigation in ambulatory settings. Participants were in contact with the electrodes for at least five minutes before the experiment started. Subsequently, the EDA recording was conducted iteratively with each pair of the six test electrodes. The procedure involved the participant placing the distal phalanx of their middle finger on the printed test electrode connected to the positive potential of the twin EDA sensor. Simultaneously, the distal phalanx of the index finger was placed on the corresponding printed electrode of the other board, linked to the 300 k $\Omega$  reference resistor towards ground potential. A relaxation task was conducted as a baseline, during which participants were instructed to relax for a few minutes while the EDA recording commenced. The task was completed, and the recording stopped when the EDA curves of the two electrode pairs had approached a mutually consistent linear trend or a stable value, according to visual assessment. Then, the participants engaged in a breathing task, where they were told to take a fast, deep breath, hold it for a second and breathe out calmly. Four to six seconds later, this procedure was repeated a second time, and the recording was stopped thereafter.

Then, the participant was asked to take a finger-sized button provided on the table with their dominant hand, which was not attached to any electrodes. The participant was instructed that an audio track would be played on which tones of two different pitches would be heard. The track would start with deep tones; whenever a high tone appeared, the participant was asked to press the button as fast as possible. In later iterations, the participant was reminded to press the button as soon as possible after the tone to increase his/her attention. The track was the same for all iterations and contained three tones of the higher pitch occurring after 13.5, 21.0, and 34.5 seconds. The low tone was a 1000 Hz tone, while the oddballs were 1500 Hz tones, all with a duration of 80 ms occurring at an interval of 1500 ms. EDA was recorded during all conditions. The electrodes were switched after each condition. The task was completed for all participants, and the entire procedure took approximately 60 minutes per individual.

### 3.4 Data Processing

At first, we plotted the curves of all participants for all electrode pairs and all tasks after applying a Butterworth lowpass filter with a 0.5 Hz cutoff frequency. We chose this frequency to filter out as much noise as possible while still maintaining SCRs, which have

a mean ascent time slightly larger than two seconds [6]. Hence, a cutoff frequency of 0.5 Hz should preserve these changes. Besides, we divided the curves by their mean before plotting to map them all in a comparable range while preserving their variance. For the oddball task, we marked the times of occurring oddballs with vertical lines. In addition, we plotted the oddball task curves after applying the first differences method subsequent to filtering and standard score normalization. This method is often used to reduce the time dependency of a non-stationary time series as an EDA measurement by mapping each data point according to the following formula:

$$x'_t = x_t - x_{t-1} \quad (1)$$

Furthermore, we used cvxEDA to split the EDA curves into phasic and tonic components for the purpose of visual inspection. cvxEDA takes a parameter called alpha, a “penalization for the sparse SMNA (sudomotor nerve activity) driver”<sup>3</sup>, which controls how many deflections in the curve are classified as SCRs. We set this parameter to 0.16 as this value seemed to achieve the best results for the curves in our plots. All other parameters were set to their default value. Since cvxEDA does not require any data preparation before its execution, we did not apply a lowpass filter for this step. However, following the developer’s suggestion, we performed standard score normalization beforehand. We included the raw, normalized curves in translucent colors. We also used the NeuroKit2 library<sup>4</sup> to separate phasic and tonic components from the EDA data measured during the oddball task. NeuroKit2 also detects SCR onsets and peaks, which we will use to further analyze the oddball task. For plotting this data, we have again used a lowpass-filter with 0.5 Hz cutoff frequency and divided the curves by their mean before passing the measurements to NeuroKit2 to obtain comparable results. The determined phasic components were additionally standard score normalized before plotting for the purpose of better comparability. We calculate the Pearson correlation between the commercial and 3D-printed electrodes.

### 3.5 Results

**3.5.1 General Observations.** We observed that the initial skin conductance values measured by all printed test electrodes were high and exhibited a decreasing trend in the first 20-30 seconds, following a decaying curve. Beyond 30-40 seconds, the Protopasta test electrode curves appeared to align with the corresponding reference curves, as evidenced by simultaneous peaks in both. In the context of the breathing task, we frequently identified two prominent peaks in the reference curves, consistent with expectations after each breath. These peaks were accompanied by additional higher-frequency fluctuations. In many cases, the Protopasta curves mirror

<sup>3</sup><https://github.com/lciti/cvxEDA> – last accessed 2024-01-25

<sup>4</sup><https://github.com/neuropsychology/NeuroKit> – last accessed 2024-01-25

**Table 2: We measure the accuracy of identified SCRs by assessing precision, which indicates the proportion of correct detections. We also evaluate recall, which signifies the proportion of actual SCRs that were successfully detected. The F1 score, derived from precision and recall, is then calculated. Bold values indicate the highest classification values.**

Electrode	Circular	Large Circular	Dome	Tall Conic	Small Conic	Inset
Precision	.430	<b>.437</b>	.393	.378	.414	.385
Recall	.475	.735	.561	<b>.903</b>	.594	.696
F1 Score	.415	<b>.608</b>	.420	.505	.483	.481

these major peaks. The oddball task curves displayed increased fluctuations, with peaks often appearing seconds after the marked oddball times, aligning with our anticipated orienting responses. These peaks were also evident in the first differences plots, although with more fluctuations.

**3.5.2 Correlation Between 3D-Printed and Commercial Electrodes.** Table 1 summarizes the results of the Pearson correlation between the six different 3D-printed electrode shapes (see Figure 1) and the commercial EDA sensor. Notably, tall conic electrodes exhibited the highest values for these metrics, followed by dome and small conic electrodes. Conversely, large circular, inset, and circular electrodes demonstrated the lowest values, although all values remained greater than one. Regarding the scaling factor, inset electrodes recorded the lowest conductivity values (10.732 for the breathing task and 11.915 for the oddball task).

Tall conic electrodes showed the highest scaling factor values (48.450 for breathing and 55.005 for oddball tasks), followed by dome and small conic electrodes. Pearson’s  $r$ , utilized to measure the resemblance of the test electrode curves to the reference curves, reached its peak with large circular electrodes (0.397 for breathing and 0.683 for the oddball task). The small conic and dome electrodes achieved high  $r$  values solely in the breathing task, while circular and tall conic electrodes secured high  $r$  values in the oddball task. All Protospasta electrodes yielded positive  $r$  values in both tasks.

Upon applying the first differences method to the curves, circular electrodes exhibited the highest fraction of relative range, the highest fraction of relative standard deviation, and the second-highest  $r$  value. Small conic and inset electrodes demonstrated the lowest fraction of relative range. Negative signs in this column resulted from negative mean values of the first differences, which can be disregarded for comparison. It’s essential to note that the first difference values indicate changes between data points. Therefore, a high fraction of relative range or fraction of relative standard deviation signifies numerous changes in the measurement curves, not skin conductances far from the mean conductance as observed in other tables. The finite differences  $r$  values exhibited similar behavior to the overall oddball task  $r$  values.

**3.5.3 EDA Classification.** We quantify how many of the detected SCRs were correct (i.e., precision), how many SCRs that occurred were detected (i.e., recall), and calculate the F1 using precision and recall. Table 2 summarizes the findings. Following the computation of the mean across a broad spectrum of frequencies, all electrodes demonstrated similar precision. However, notable distinctions emerged in recall values: tall conic electrodes exhibited

significantly high recall (0.903). Subsequently, large circular and inset electrodes recorded the next highest recall values. Large circular electrodes also attained the highest F1 score (0.608). Circular and dome electrodes registered the lowest F1 score. Observations regarding latency revealed that small conic and dome electrode SCRs exhibited the longest latency, while circular seemed to capture SCRs earlier than the reference electrodes, indicated by the negative sign. Regarding SCR amplitudes, tall conic electrodes measured the largest, while circular electrodes measured the lowest. Notably, all test electrodes demonstrated positive mean amplitude relative differences, implying that, after normalization by the curve means, they measured larger SCRs than the reference electrodes. Mean latency shift and amplitude mean relative difference was computed based solely on SCRs occurring in oddball windows where both the test and reference measurements captured an SCR. Conversely, absolute latencies and amplitudes provided on a white background encompassed all SCRs in oddball windows, irrespective of whether the corresponding pair of electrodes had also recorded an SCR.

## 4 DISCUSSION

We have proposed a method to incorporate EDA sensors into 3D-printed objects. Our focus in this research has been on employing simple measurement techniques, specifically the quasi-constant current and voltage methods, as well as the constant current and voltage method using DC. Two primary reasons guided our choice of these methods. Firstly, they are likely to be seamlessly integrated into devices with limited space requirements, such as most mobile devices, a focus shared by the papers highlighted in section 3.2. Secondly, these methods provide a foundation for further development. Our approach involved using circuits to measure the output voltage with a microcontroller. Alternatively, analog signal processing could be implemented in hardware, as Zhao et al. [41] demonstrated, who employed binary signal classification. More specialized data preparation circuitry could be added, similar to our study, where we incorporated amplification, such as segregating into phasic and tonic components. Examining sensor designs and the conducted study should be considered a proof of concept, offering a starting point for future investigations into integrating EDA sensors into 3D prints or for practical hands-on projects. We propose certain recommendations regarding the selection of electrode shapes. It is advisable to utilize electrodes with a larger skin contact area to achieve improved accuracy for SCRs. A flat-shaped electrode is recommended when low contact resistances are a priority. A pointed shape may be employed if the objective is to attain heightened sensitivity. In cases where robustness is crucial, particularly in applications where EDA recording may be susceptible

to motion interference, electrodes with an inwardly curved shape prove advantageous. The inwardly curved electrodes yield stable results with reasonably high accuracy and provide a secure grip due to their geometry. Additionally, it is essential to consider a polarization time of approximately 30 to 40 seconds [4].

## 5 CONCLUSION AND FUTURE WORK

This paper investigates the application of 3D-printed electrodes for measuring Electrodermal Activity (EDA) and assesses how electrode shape impacts measurement accuracy. We tested six 3D-printed electrodes with a conductive filament in a user study with six participants compared to commercially available off-the-shelf nickel electrodes. The results show that printed electrodes maintain EDA measurement accuracy, with the best performance from electrodes with a flat shape and a large diameter. The findings suggest potential applications in everyday objects like tools, devices, cups, steering wheels, and wristbands, facilitating ambulatory EDA recording without cables or adhesive electrodes. The paper's contribution paves the way for integrating EDA sensors into various everyday objects through 3D printing, enabling broader accessibility and application of EDA measurement in diverse contexts. The work suggests future research directions, including exploring other materials for printed electrodes, optimizing algorithm parameters for specific electrode shapes, and designing systems utilizing EDA as an input modality.

## REFERENCES

- [1] Antonio Affanni, Giovanni Chiorboli, et al. 2014. Wearable instrument for skin potential response analysis in AAL applications. In *Proceedings of the 20th IMEKO TC4 Symposium on Measurements of Electrical Quantities: Research on Electrical and Electronic Measurement for the Economic Upturn, Together with 18th TC4 International Workshop on ADC and DCA Modeling and Testing, IWADC*.
- [2] Aljawharah A. Alsharif, Nataly S. Milan Cucuri, Rishabh B. Mishra, and Nazek El-Atab. 2023. 3D Printed Dry Electrodes for Electrophysiological Signal Monitoring: A Review. *Advanced Materials Technologies* 8, 7 (2023), 2201677. <https://doi.org/10.1002/admt.202201677> arXiv:<https://onlinelibrary.wiley.com/doi/pdf/10.1002/admt.202201677>
- [3] Yadid Ayzenberg, Javier Hernandez Rivera, and Rosalind Picard. 2012. FEEL: Frequent EDA and Event Logging – a Mobile Social Interaction Stress Monitoring System. In *CHI '12 Extended Abstracts on Human Factors in Computing Systems* (Austin, Texas, USA) (CHI EA '12). Association for Computing Machinery, New York, NY, USA, 2357–2362. <https://doi.org/10.1145/2212776.2223802>
- [4] Ebrahim Babaei, Benjamin Tag, Tilman Dinger, and Eduardo Velloso. 2021. A Critique of Electrodermal Activity Practices at CHI. In *Proceedings of the 2021 CHI Conference on Human Factors in Computing Systems* (Yokohama, Japan) (CHI '21). Association for Computing Machinery, New York, NY, USA, Article 177, 14 pages. <https://doi.org/10.1145/3411764.3445370>
- [5] Ravi Bhoja, Oren T Guttman, Amanda A Fox, Emily Melikman, Matthew Kosemund, and Kevin J Gingrich. 2020. Psychophysiological stress indicators of heart rate variability and electrodermal activity with application in healthcare simulation research. *Simulation in Healthcare* 15, 1 (2020), 39–45. <https://doi.org/10.1097/SIH.0000000000000402>
- [6] Wolfram Boucsein. 2012. *Electrodermal activity*. Springer Science & Business Media.
- [7] Francesco Chiossi, Thomas Kosch, Luca Menghini, Steeven Villa, and Sven Mayer. 2023. SensCon: Embedding Physiological Sensing into Virtual Reality Controllers. *Proc. ACM Hum.-Comput. Interact.* 7, MCHI, Article 223 (sep 2023), 32 pages. <https://doi.org/10.1145/3604270>
- [8] Francesco Chiossi, Yagiz Turgut, Robin Welsch, and Sven Mayer. 2023. Adapting Visual Complexity Based on Electrodermal Activity Improves Working Memory Performance in Virtual Reality. *Proc. ACM Hum.-Comput. Interact.* 7, MCHI, Article 196 (sep 2023), 26 pages. <https://doi.org/10.1145/3604243>
- [9] Jose C Conchell and Javier Calpe. 2018. Design Development and Evaluation of a System to Obtain Electrodermal Activity. *Analog Devices*. Available online: <https://www.analog.com/media/en/technical-documentation/tech-articles/design-development-and-evaluation-of-a-system-to-obtain-electrodermal-activity.pdf> (accessed on 2 May 2022) (2018).
- [10] A. Dijkshoorn, P. Werkman, M. Welleweerd, G. Wolterink, B. Eijking, J. Delamare, R. Sanders, and G. J. M. Krijnen. 2018. Embedded sensing: integrating sensors in 3-D printed structures. *Journal of Sensors and Sensor Systems* 7, 1 (2018), 169–181. <https://doi.org/10.5194/jsss-7-169-2018>
- [11] Society for Psychophysiological Research Ad Hoc Committee on Electrodermal Measures. 2012. Publication recommendations for electrodermal measurements. *Psychophysiology* 49, 8 (2012), 1017–1034. <https://doi.org/10.1111/j.1469-8986.2012.01384.x> arXiv:<https://onlinelibrary.wiley.com/doi/pdf/10.1111/j.1469-8986.2012.01384.x>
- [12] DONC Fowles. 1981. Committee report publication recommendations for electrodermal. *Psychophysiology* 18 (1981), 232–239.
- [13] Dong Hae Ho, Panuk Hong, Joong Tark Han, Sang-Youn Kim, S. Joon Kwon, and Jeong Ho Cho. 2020. 3D-Printed Sugar Scaffold for High-Precision and Highly Sensitive Active and Passive Wearable Sensors. *Advanced Science* 7, 1 (2020), 1902521. <https://doi.org/10.1002/advs.201902521> arXiv:<https://onlinelibrary.wiley.com/doi/pdf/10.1002/advs.201902521>
- [14] Arthur S. P. Jansen, Xay Van Nguyen, Vladimir Karpitskiy, Thomas C. Mettenleiter, and Arthur D. Loewy. 1995. Central Command Neurons of the Sympathetic Nervous System: Basis of the Fight-or-Flight Response. *Science* 270, 5236 (1995), 644–646. <https://doi.org/10.1126/science.270.5236.644> arXiv:<https://www.science.org/doi/pdf/10.1126/science.270.5236.644>
- [15] Krisztian Kasos, Zoltan Kekecs, Luca Csirmaz, Szabolcs Zimonyi, Fanni Vikor, Eniko Kasos, Andras Veres, Eszter Kotyuk, and Anna Szekeley. 2020. Bilateral comparison of traditional and alternate electrodermal measurement sites. *Psychophysiology* 57, 11 (2020), e13645. <https://doi.org/10.1111/psyp.13645> arXiv:<https://onlinelibrary.wiley.com/doi/pdf/10.1111/psyp.13645>
- [16] Vassiliki Katseli, Anastasios Economou, and Christos Kokkinos. 2019. Single-step fabrication of an integrated 3D-printed device for electrochemical sensing applications. *Electrochemistry Communications* 103 (2019), 100–103. <https://doi.org/10.1016/j.elecom.2019.05.008>
- [17] Christopher Changmok Kim, Jiawen Han, Dingding Zheng, George Chernyshov, and Kai Kunze. 2021. Using Smart Eyewear to Sense Electrodermal Activity While Reading. In *Adjunct Proceedings of the 2021 ACM International Joint Conference on Pervasive and Ubiquitous Computing and Proceedings of the 2021 ACM International Symposium on Wearable Computers (Virtual, USA) (UbiComp/ISWC '21 Adjunct)*. Association for Computing Machinery, New York, NY, USA, 472–475. <https://doi.org/10.1145/3460418.3479356>
- [18] Madison Klarkowski, Daniel Johnson, Peta Wyeth, Cody Phillips, and Simon Smith. 2018. Don't Sweat the Small Stuff: The Effect of Challenge-Skill Manipulation on Electrodermal Activity. In *Proceedings of the 2018 Annual Symposium on Computer-Human Interaction in Play (CHI PLAY '18)*. Association for Computing Machinery, New York, NY, USA, 231–242. <https://doi.org/10.1145/3242671.3242714>
- [19] Thomas Kosch, Jakob Karolus, Havy Ha, and Albrecht Schmidt. 2019. Your Skin Resists: Exploring Electrodermal Activity as Workload Indicator during Manual Assembly. In *Proceedings of the ACM SIGCHI Symposium on Engineering Interactive Computing Systems (Valencia, Spain) (EICS '19)*. Association for Computing Machinery, New York, NY, USA, Article 8, 5 pages. <https://doi.org/10.1145/3319499.3328230>
- [20] Thomas Kosch, Jakob Karolus, Johannes Zagermann, Harald Reiterer, Albrecht Schmidt, and Pawel W. Woźniak. 2023. A Survey on Measuring Cognitive Workload in Human-Computer Interaction. *ACM Comput. Surv.* 55, 13s, Article 283 (jul 2023), 39 pages. <https://doi.org/10.1145/3582272>
- [21] Yun Liu and Siquing Du. 2018. Psychological stress level detection based on electrodermal activity. *Behavioural Brain Research* 341 (2018), 50–53. <https://doi.org/10.1016/j.bbr.2017.12.021>
- [22] Mary L. Mahon and William G. Iacono. 1987. Another Look at the Relationship of Electrodermal Activity to Electrode Contact Area. *Psychophysiology* 24, 2 (1987), 216–222. <https://doi.org/10.1111/j.1469-8986.1987.tb00280.x> arXiv:<https://onlinelibrary.wiley.com/doi/pdf/10.1111/j.1469-8986.1987.tb00280.x>
- [23] Karola Marky, Andreas Weiß, Andrii Matvienko, Florian Brandherm, Sebastian Wolf, Martin Schmitz, Florian Krell, Florian Müller, Max Mühlhäuser, and Thomas Kosch. 2021. Let's Frets! Assisting Guitar Students During Practice via Capacitive Sensing. In *Proceedings of the 2021 CHI Conference on Human Factors in Computing Systems (CHI '21)*. Association for Computing Machinery, New York, NY, USA, Article 746, 12 pages. <https://doi.org/10.1145/3411764.3445595>
- [24] Karola Marky, Andreas Weiß, Florian Müller, Martin Schmitz, Max Mühlhäuser, and Thomas Kosch. 2021. Let's Frets! Mastering Guitar Playing with Capacitive Sensing and Visual Guidance. In *Extended Abstracts of the 2021 CHI Conference on Human Factors in Computing Systems (CHI EA '21)*. Association for Computing Machinery, New York, NY, USA, Article 169, 4 pages. <https://doi.org/10.1145/3411763.3451536>
- [25] Sander Nieuwenhuis, Eco J. De Geus, and Gary Aston-Jones. 2011. The anatomical and functional relationship between the P3 and autonomic components of the orienting response. *Psychophysiology* 48, 2 (2011), 162–175. <https://doi.org/10.1111/j.1469-8986.2010.01057.x> arXiv:<https://onlinelibrary.wiley.com/doi/pdf/10.1111/j.1469-8986.2010.01057.x>

- [26] Matthew K.X.J. Pan, Gordon Jih-Shiang Chang, Gokhan H. Himmetoglu, AJung Moon, Thomas W. Hazelton, Karon E. MacLean, and Elizabeth A. Croft. 2011. Galvanic Skin Response-Derived Bookmarking of an Audio Stream. In *CHI '11 Extended Abstracts on Human Factors in Computing Systems* (Vancouver, BC, Canada) (CHI EA '11). Association for Computing Machinery, New York, NY, USA, 1135–1140. <https://doi.org/10.1145/1979742.1979716>
- [27] Terence W Picton et al. 1992. The P300 wave of the human event-related potential. *Journal of clinical neurophysiology* 9 (1992), 456–456.
- [28] Ming-Zher Poh, Nicholas C. Swenson, and Rosalind W. Picard. 2010. A Wearable Sensor for Unobtrusive, Long-Term Assessment of Electrodermal Activity. *IEEE Transactions on Biomedical Engineering* 57, 5 (2010), 1243–1252. <https://doi.org/10.1109/TBME.2009.2038487>
- [29] Gunnar C. Pope and Ryan J. Halter. 2019. Design and Implementation of an Ultra-Low Resource Electrodermal Activity Sensor for Wearable Applications. *Sensors* 19, 11 (2019). <https://doi.org/10.3390/s19112450>
- [30] Nasuha Rohaizad, Carmen C. Mayorga-Martinez, Filip Novotný, Richard D. Webster, and Martin Pumera. 2019. 3D-printed Ag/AgCl pseudo-reference electrodes. *Electrochemistry Communications* 103 (2019), 104–108. <https://doi.org/10.1016/j.elecom.2019.05.010>
- [31] P. Salvo, R. Raedt, E. Carrette, D. Schaubroeck, J. Vanfleteren, and L. Cardon. 2012. A 3D printed dry electrode for ECG/EEG recording. *Sensors and Actuators A: Physical* 174 (2012), 96–102. <https://doi.org/10.1016/j.sna.2011.12.017>
- [32] M. Schmidt, D. Penner, A. Burkl, R. Stojanovic, T. Schümann, and P. Beckerle. 2016. Implementation and evaluation of a low-cost and compact electrodermal activity measurement system. *Measurement* 92 (2016), 96–102. <https://doi.org/10.1016/j.measurement.2016.06.007>
- [33] Yu Shi, Natalie Ruiz, Ronnie Taib, Eric Choi, and Fang Chen. 2007. Galvanic Skin Response (GSR) as an Index of Cognitive Load. In *CHI '07 Extended Abstracts on Human Factors in Computing Systems* (San Jose, CA, USA) (CHI EA '07). Association for Computing Machinery, New York, NY, USA, 2651–2656. <https://doi.org/10.1145/1240866.1241057>
- [34] Jainendra Shukla, Miguel Barreda-Ángeles, Joan Oliver, G. C. Nandi, and Domènec Puig. 2021. Feature Extraction and Selection for Emotion Recognition from Electrodermal Activity. *IEEE Transactions on Affective Computing* 12, 4 (2021), 857–869. <https://doi.org/10.1109/TAFFC.2019.2901673>
- [35] David A. T. Sidle and Peter A. Heron. 1976. Effects of Length of Training and Amount of Tone Frequency Change on Amplitude of Autonomic Components of the Orienting Response. *Psychophysiology* 13, 4 (1976), 281–287. <https://doi.org/10.1111/j.1469-8986.1976.tb03076.x> arXiv:<https://onlinelibrary.wiley.com/doi/pdf/10.1111/j.1469-8986.1976.tb03076.x>
- [36] Nancy K Squires, Kenneth C Squires, and Steven A Hillyard. 1975. Two varieties of long-latency positive waves evoked by unpredictable auditory stimuli in man. *Electroencephalography and Clinical Neurophysiology* 38, 4 (1975), 387–401. [https://doi.org/10.1016/0013-4694\(75\)90263-1](https://doi.org/10.1016/0013-4694(75)90263-1)
- [37] Ivo V Stuldreher, Nattapong Thammasan, Jan B F van Erp, and Anne-Marie Brouwer. 2020. Physiological synchrony in EEG, electrodermal activity and heart rate reflects shared selective auditory attention. *Journal of Neural Engineering* 17, 4 (aug 2020), 046028. <https://doi.org/10.1088/1741-2552/aba87d>
- [38] D.J. van der Mee, M.J. Gevonden, J.H.D.M. Westerink, and E.J.C. de Geus. 2021. Validity of electrodermal activity-based measures of sympathetic nervous system activity from a wrist-worn device. *International Journal of Psychophysiology* 168 (2021), 52–64. <https://doi.org/10.1016/j.ijpsycho.2021.08.003>
- [39] Gerjan Wolterink, Pedro Dias, Remco G. P. Sanders, Frodo Muijzer, Bert-Jan van Beijnum, Peter Veltink, and Gijs Krijnen. 2020. Development of Soft sEMG Sensing Structures Using 3D-Printing Technologies. *Sensors* 20, 15 (2020). <https://doi.org/10.3390/s20154292>
- [40] Yuanxuan Xu, Xiaoyue Wu, Xiao Guo, Bin Kong, Min Zhang, Xiang Qian, Shengli Mi, and Wei Sun. 2017. The Boom in 3D-Printed Sensor Technology. *Sensors* 17, 5 (2017). <https://doi.org/10.3390/s17051166>
- [41] Haibin Zhao, Alexander Scholz, Michael Beigl, Si Ni, Surya Abhishek Singaraju, and Jasmin Aghassi-Hagmann. 2022. Printed Electrodermal Activity Sensor with Optimized Filter for Stress Detection. In *Proceedings of the 2022 ACM International Symposium on Wearable Computers* (Cambridge, United Kingdom) (ISWC '22). Association for Computing Machinery, New York, NY, USA, 112–114. <https://doi.org/10.1145/3544794.3558479>